Efficiency Maps of Electrical Machines

Amin Mahmoudi, Wen L. Soong
School of Electrical and Electronic Engineering
University of Adelaide, Australia
amaminmahmoudi@gmail.com
wen.soong@adelaide.edu.au

Gianmario Pellegrino, Eric Armando
Politecnico di Torino, Corso Duca degli
Abruzzi 24, Torino, 10129 Italy
gianmario.pellegrino@polito.it
eric.armando@polito.it

Abstract— **This paper investigates the calculation, modelling and interpretation of efficiency maps for electrical machines. The efficiency maps are calculated using a finite-element based mapping of losses, torque and flux-linkage as a function of the *d*- and *q*-axis currents and speed. For modelling efficiency maps, it is shown that a number of key loss types can be described in the form $T^m \omega^n$. The effect of each of these losses on the shape of the efficiency map is then explored. It is found that practical efficiency maps can be approximated using a series of such terms which leads to a better understanding of the losses in the machine. The above results are validated using the loss and efficiency maps of three example machines.**

I. INTRODUCTION

A. Energy Efficiency of Traction Drives

Traction drives are the main propulsion drives for electric and hybrid vehicles and other transportation applications such as ships and trains. They need to operate as efficiently as possible to maximise the vehicle driving range. The accepted means for evaluating vehicle energy efficiency is to examine its performance over standard driving cycles. A driving cycle is a representative vehicle velocity versus time profile. There are different driving cycles for urban and highway driving. Fig. 1a shows four example standard driving cycles for vehicles.

Based on assumed vehicle characteristics, gear ratios and control strategy, the required instantaneous electric machine torque and speed to meet the driving cycle can be calculated [1]. A scatter plot of these instantaneous torque and speed requirements are plotted in Fig. 1b for one of the driving cycles in Fig. 1a assuming different gearing ratios. This example illustrates that under normal driving conditions, the motor spends little time at its maximum output power, but rather, most of its time at intermediate torque and speed points.

An efficiency map for an electric machine is a contour plot of the electrical machine efficiency on axes of torque and speed. It describes the maximum efficiency for any speed/torque combination and is a convenient way to represent the motor drive over a range of operating points defined by a driving cycle.

Using the instantaneous torque/speed operating points shown in Fig. 1b and the efficiency map, the electrical input power for every operating point can be obtained by dividing the mechanical output power (that is, the product of torque

and speed) by the efficiency at the corresponding point. The energy consumption of the traction drive can be estimated by integrating the electrical input power over the driving cycle. Consequently, in order to improve the efficiency of a vehicle for a certain driving cycle, the motor maximum efficiency should be designed to cover its regular working area.

The dashed lines in Fig. 1b show the torque-speed capability of the motor drive demonstrating its two operating modes: constant torque at low speeds and constant power at high speeds.

When considering the design of motor drives, though the efficiency of the drive is affected by both the efficiency of the inverter and of the electric motor, there is generally greater attention focused on the efficiency of the electric machine. This is because the efficiency of electric machines is normally lower than inverters and shows a greater variability with operating point and type of machine.
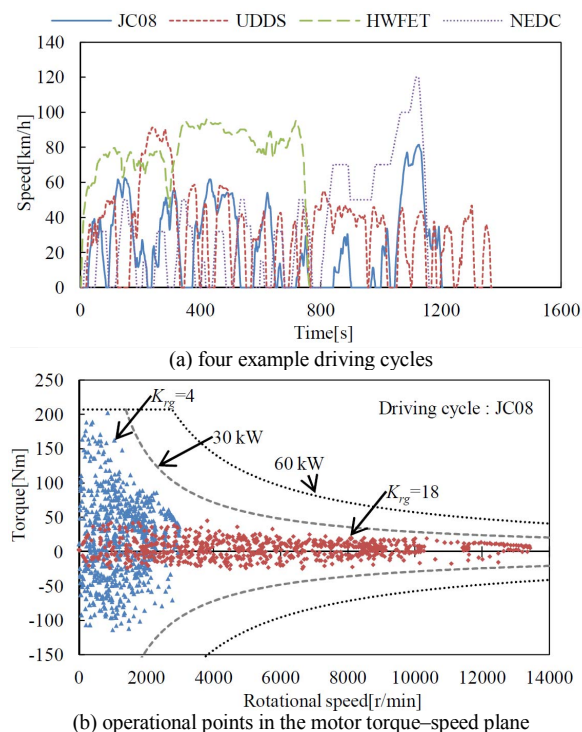

(a) four example driving cycles

(b) operational points in the motor torque–speed plane

Figure 1.   Example driving cycles and the resultant operational points [1].

2791

B. Efficiency Maps of Electric Machines

Permanent magnet machines are the primary type of traction machine used for commercial electric and hybrid passenger vehicles. This is because they offer a combination of high torque density (small size) and high efficiency which is difficult to surpass with other motor types.

Permanent magnet (PM) electric machines normally use d- and q-axis current control to achieve smooth torque control and fast dynamic response. The two key motor control variables are the d-axis stator current I_d and the q-axis stator current I_q. The two main operating constraints are the machine voltage limit, set by either the inverter voltage capability or the battery voltage, and the machine current limit, set by either the inverter current capability or the motor thermal limit.

The machine efficiency map is obtained by finding the maximum efficiency for each torque T and speed ω combination in the motor torque-speed plane. For example at the desired speed, the combinations of the two control parameters I_d and I_q, which produce the desired torque are examined. Then the combination is found which yields the highest efficiency while satisfying the machine voltage and current limit.

C. Problem Statement

In the context of electrical machines, efficiency maps have been mainly used in the drive design of electrical and hybrid vehicles. For instance, efficiency maps are useful to compare the performance of different motor types [1-3]. There has however been little work done on interpreting and modelling efficiency maps.

The key novel contribution of this work is the description of the power loss of the electrical machine at a given torque T and speed ω as the sum of loss terms of the form $T^m\omega^n$ where m and n are integers. The details of the electrical machine modelling under constant torque and constant power operation is presented in Section II. Section III then describes the calculation of three example efficiency maps and Section IV examines their characteristics. Section V describes the modelling of the calculated efficiency maps using loss terms and Section VI describes some preliminary results from experimental measurements of efficiency maps.

II. THEORETICAL BASIS OF LOSS FUNCTIONS

It is proposed that the power loss P_{loss} in an electrical machine can be expressed in the form,

$$P_{loss}(T,\omega) = \sum k_{mn} T^m \omega^n \qquad (1)$$

for integers m and n, and constants k_{mn}. This concept has a solid physical basis. For example, consider a simple loss model for a surface PM machine under maximum-torque-per-ampere operation. The no-load (eddy-current) iron loss is proportional to ω^2. The torque is proportional to current and hence stator copper loss is proportional to T^2. Thus to a first approximation its loss can be described as,

$$P_{loss}(T,\omega) = k_{20}T^2 + k_{02}\omega^2 \qquad (2)$$

The following simplified machine analysis, applicable to induction (IM), surface PM (SPM) and interior PM (IPM) machines, will be used for the loss function analysis during the constant-torque and constant-power operating regions.

Consider that the machine has two stator current components: a flux-producing current I_F and a torque-producing current I_T. The total stator current $I = \sqrt{(I_T^2 + I_F^2)}$ and with a stator resistance R, the stator copper loss is $3I^2R$.

The main flux Φ in the machine is a function of the flux-producing current I_F. For induction machines it is given by $\Phi \propto I_F$, while for PM machines $\Phi \propto I_{PM} - I_F$ where the equivalent current I_{PM} represents the PM flux. The induced voltage in the machine V is proportional to $\Phi\omega$.

The stator iron loss, taking only the main (fundamental) flux Φ into account, is proportional to $\Phi^2\omega^2$ (eddy-current loss) and $\Phi^2\omega$ (hysteresis loss). This ignores the armature reaction flux associated with the torque-producing current.

The torque T, produced by the machine, is a function of the torque-producing and the flux-producing currents: for induction machines: $T \propto \Phi \times I_T \propto I_F I_T$, while for PM machines $T \propto k_1 I_T + k_2 I_F I_T$ (ignoring saturation effects).

Using this modelling approach and many simplifying approximations for the machine control and performance, the key loss terms of the form $k_{mn}T^m\omega^n$ can be identified. These are summarized in Table I as a 4-4 matrix for k_{mn} for m and n values between 0 and 3. Both the constant torque and constant power regions are examined for each machine. The following terms are used in the table: copper losses in the stator (cu-s) and rotor (cu-r), iron loss (fe), magnet losses (mgnt) and windage losses (wdge).

In the constant torque region, the main copper loss term is $k_{20}T^2$ and the main iron loss term is $k_{02}\omega^2$. Windage losses appear as $k_{03}\omega^3$. In the constant power region, the key loss type depends on the machine type: copper losses for the IM, iron losses for the IPM and magnet losses for the SPM.

Fig. 2a shows a 4-4 matrix of contour plots for power loss terms $k_{mn}T^m\omega^n$ as a function of torque and speed. The lower left term $k_{00}T^0\omega^0$ is a constant while the left most column represents terms related to only torque and the lowest row represents terms related to only speed. The top right plot refers to $k_{33}T^3\omega^3$.

Fig. 2b shows the shape of the efficiency plots corresponding to each single loss term in Fig. 2a. The relationship between each loss term $T^m\omega^n$ and the resultant efficiency map is given by,

$$\eta = \frac{T\omega}{T\omega + T^m\omega^n} = \frac{1}{1 + T^{m-1}\omega^{n-1}} \approx 1 - T^{m-1}\omega^{n-1} \qquad (3)$$

for small values of $T^{m-1}\omega^{n-1}$. Thus the shape of the efficiency plots is similar to that of the loss plots one row down and one column left. The natural "centre" of plots is the $k_{11}T\omega$ plot which corresponds to a constant value of efficiency at all operating points. For all the other efficiency maps in the matrix, the highest efficiency is the point or line closest to this "centre" plot. In addition, the further a given plot is from the "centre" plot, the steeper the efficiency gradient within that plot.
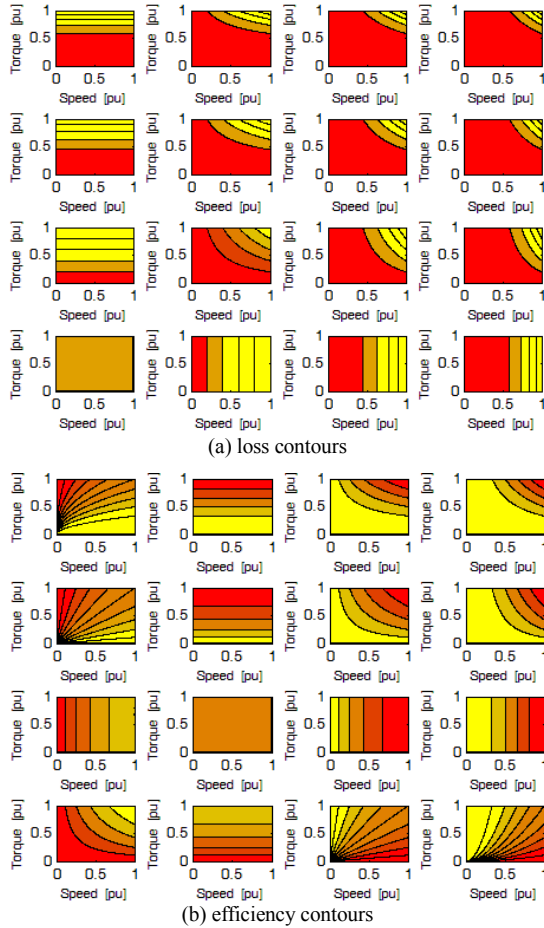
2792

TABLE I. PREDICTED ANALYTICAL LOSS FUNCTIONS

Induction								
	Constant Torque				Constant Power			
T^3								
T^2	cu-s	cu-r	fe				cu-s/r	
T	cu-s		fe		fe	cu-r	cu-s	
1	cu-s		fe	wdge	fe			wdge
	1	ω	ω^2	ω^3	1	ω	ω^2	ω^3

Interior PM								
	Constant Torque				Constant Power			
T^3								
T^2	cu-s	fe	fe		cu-s			
T	cu-s							
1		fe	fe	wdge	cu/fe		fe	wdge
	1	ω	ω^2	ω^3	1	ω	ω^2	ω^3

Surface PM								
	Constant Torque				Constant Power			
T^3								
T^2	cu-s		mgnt		cu-s		mgnt	
T								
1		fe	fe	wdge	cu/fe		mgnt	wdge
	1	ω	ω^2	ω^3	1	ω	ω^2	ω^3

(a) loss contours

(b) efficiency contours

Figure 2. Contour plots of power loss (a) and efficiency (b) on axes of torque versus speed for loss terms of the form $k_{mn}T^m\omega^n$ where m and n are each between 0 and 3.

III. FINITE-ELEMENT CALCULATION OF EFFICIENCY MAPS

A. Three Example 50-kW, 12-kr/min Machine Designs

Three example machines designed for a traction application are compared. An induction motor (IM), interior permanent magnet motor (IPM) and surface permanent magnet (SPM) motor design for the same 50-kW, 12-kr/min electric traction application were considered [7]. Their cross-sections are shown in Fig. 3. All machines have the same stack length and stator outer diameter. The key parameters of the motors are reported in Table II.

Finite-element analysis was used to predict their performance characteristics [7], including the maximum torque versus speed capability envelope and the contour plots of the minimum loss and maximum efficiency for any torque versus speed operating point within this envelope.
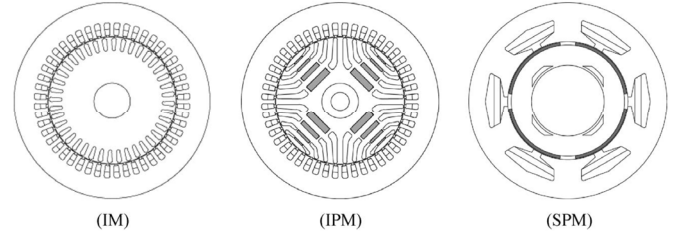

(IM)　　　　(IPM)　　　　(SPM)

Figure 3. Cross-sections of the three machines [7]

TABLE II. SPECIFICATIONS OF THREE 50-KW, 12 KR/MIN MOTORS

	IM	IPM	SPM
Key Dimensions			
- stator outer diameter		216 mm	
- airgap length		0.7 mm	
- stack length		170 mm	
Design Parameters			
- poles	4	4	4
- stator slots	48	48	6
- slots per pole per phase (SPP)	4	4	0.5
- copper slot fill (copper/slot area)	40%	40%	40%
Mechanical Parameters			
- continuous torque at 3.2 kW loss	110 Nm	160 Nm	130 Nm
- rated speed at continuous torque	4.0 kr/min	3.8 kr/min	3.8 kr/min
- overload torque capability	210 Nm	210 Nm	150 Nm
Electrical Parameters			
- rated voltage (rms line)	212 V	212 V	212 V
- back-emf at 12 krpm (20°C)	-	0.98 pu	3.12 pu
- characteristic current (rms 150°C)	-	145 A	136 A
- stator resistance (150°C)	27mΩ	27mΩ	21mΩ

B. Finite-Element Evaluation of Iron Loss Maps

The operating loss maps were calculated at constant speed using the Magnet/Infolytica finite-element package over the expected I_d, I_q operating range of each machine. The loss maps of the IPM machine are shown in Fig. 4 evaluated at 3,500 r/min (733 Hz).

The loss model utilized by the FEA software is of the form:

$$Loss/kg = K_h f^\alpha B^\beta + K_e f^2 B^2 \qquad (4)$$

where f [Hz] is the frequency, B [T] is the peak of flux density and coefficients K_h, α and β account for hysteresis
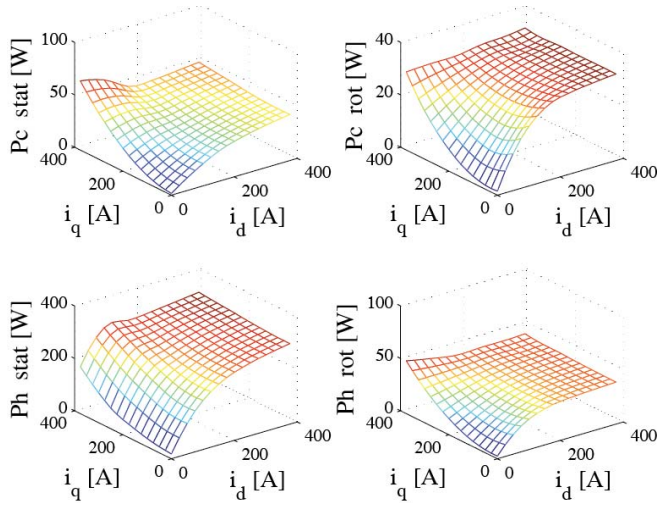
Figure 5.   Flux linkage maps for the IPM motor.

Figure 4.   Loss maps calculated at 3,500 rpm for the IPM machine over the i_d, i_q domain. *Pc* stands for eddy current loss and *Ph* for hysteresis loss.

and anomalous loss, while K_e characterizes the eddy current loss component [8]. The coefficients come from a curve fit of data loss curves provided by the steel manufacturer for tests under sinusoidal excitation. For the M250-35A steel grade considered they are: $K_e = 3.15 \times 10^{-5}$, $K_h = 0.00778$, $\alpha = 1.231$ and $\beta = 1.79$.

Harmonic fields and rotational excitation effects are taken into account in the iron loss calculations [8]. The finite-element package decomposes the local flux density waveforms into single harmonics and then superimposes the respective loss contributions according to (4).

The 3,500 rpm loss results in Fig. 4 can be scaled with speed (fundamental frequency) by application of (4). The four loss components (*Ph* stands for modified hysteresis, *Pe* stands for eddy currents) are scaled with speed as follows,

$$P_{h,stat}(i_d, i_q) = P_{h,stat,0}(i_d, i_q) \cdot \left(\frac{n}{n_0}\right)^{\alpha} \tag{5a}$$

$$P_{h,rot}(i_d, i_q) = P_{h,rot,0}(i_d, i_q) \cdot \left(\frac{n}{n_0}\right)^{\alpha} \tag{5b}$$

$$P_{e,stat}(i_d, i_q) = P_{e,stat,0}(i_d, i_q) \cdot \left(\frac{n}{n_0}\right)^{2} \tag{5c}$$

$$P_{e,rot}(i_d, i_q) = P_{e,rot,0}(i_d, i_q) \cdot \left(\frac{n}{n_0}\right)^{2} \tag{5d}$$

The subscript "0" stands for the reference speed conditions which in this case is 3,500 r/min.

C. Permanent Magnet Eddy-Current Loss

The PM loss is negligible in the IPM machine but is substantial in the SPM machine. In both cases, the magnets are considered as solid pieces of infinite length (i.e. a 2D model). For loss reduction, each pole is segmented into five tangential segments and ten axial segments. The effect of axial segmentation is analysed off-line using a reduction factor according to the shape of the final PM pieces. This final shape is 16 mm (tangentially) by 17 mm (axially). Based on this, the magnet loss is estimated at 40% of the value calculated by the 2D model [9].
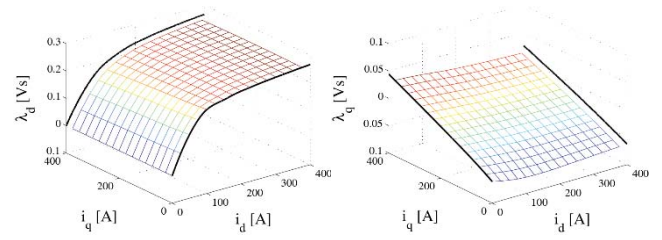
D. Determination of Rotor Bar Loss of the IM

The loss in the rotor bars is evaluated using the method described in [10]. The set of steady-state rotor bar currents corresponding to a chosen set of I_d, I_q stator components is found via a three-step static FEA procedure. The loss in the rotor cage is evaluated using the calculated bar currents, assuming an average rotor temperature of 180°C. The end connections are represented as additional lumped resistances which are calculated analytically according to the shape and dimensions of the end rings. By using this method the rotor bar loss can be mapped throughout the I_d, I_q domain in a similar fashion as was done for the core loss in Fig. 4.

E. Merging of Loss Data into Loss and Efficiency Maps

The flux linkage maps are FEA calculated,

$$\begin{cases} \lambda_d = \lambda_d(i_d, i_q) \\ \lambda_q = \lambda_q(i_d, i_q) \end{cases} \tag{6}$$

and Fig. 5 shows the IPM machine results. The torque map versus I_d, I_q is also available from FEA, or it can evaluated off-line as the external product of the current and flux linkage vectors in *dq* components.

Based on the above calculation method, the torque and loss maps over the I_d, I_q domain and at each speed are available for the three machines. Therefore, the combinations of I_d, I_q minimizing loss for each target torque and mechanical speed can be found through Matlab manipulation, and from these the control trajectories for maximum efficiency are plotted in the I_d, I_q plane. Voltage and current limits are easily imposed during this off-line manipulation. The power loss and efficiency maps reported in Fig. 6 for the three machine examples are a result of the procedure described in this section. They all refer to the same power converter size, i.e. the same voltage and current limits.

IV.   DISCUSSION OF RESULTS

Fig. 6 shows the power loss contours and the efficiency maps for the three motors in both the torque-speed and the power-speed planes. The torque-speed plane plots highlights the machine performance in the constant torque region while the power-speed plots highlight the constant power performance.

To help understand these curves, Fig. 7 shows the stator copper loss and current versus torque characteristics at standstill and Fig. 8 shows the no-load loss versus speed characteristics. These represent the axis intercepts of the torque versus speed power loss contour plots.
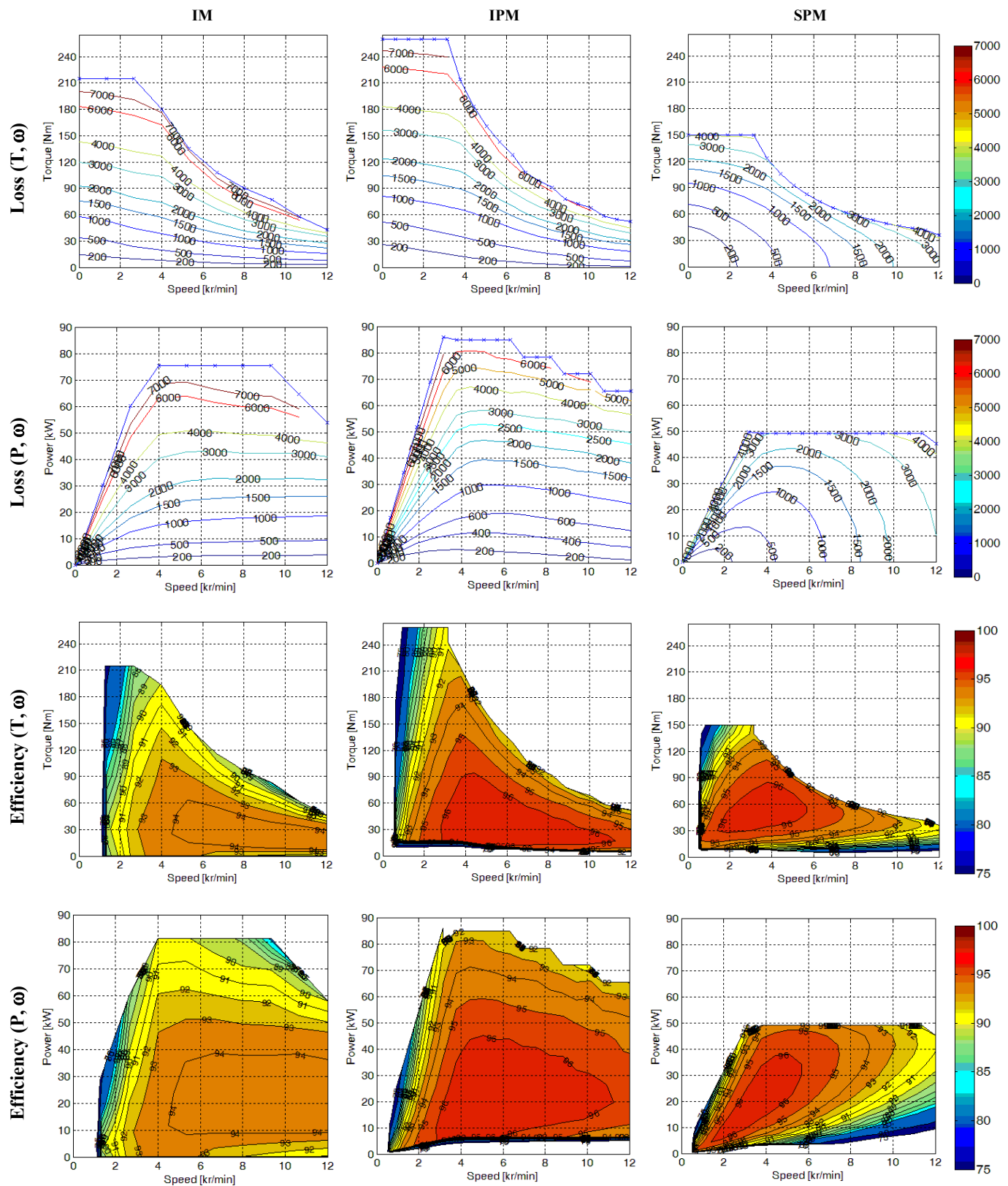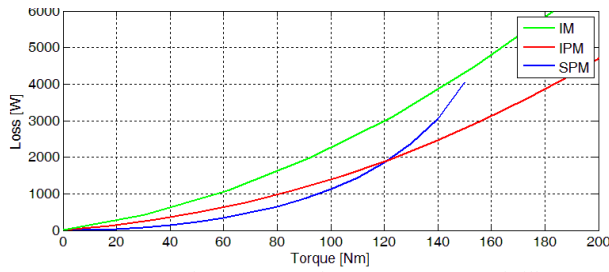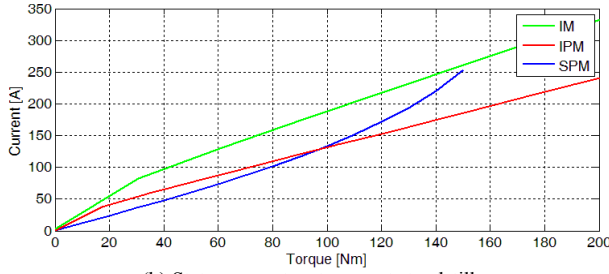
2794

Figure 6. The efficiency map shapes and their associated loss contours of the IM, IPM and SPM machines in the torque-speed and power-speed planes, under common voltage and current limits: 212 V (rms line), 255 A (rms)

2795

(a) Stator (and rotor) copper loss vs torque at standstill.

(b) Stator current vs torque at standstill

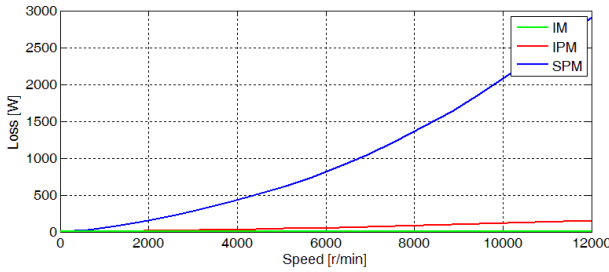Figure 7.   Power loss and current versus torque at standstill



Figure 8.   Loss vs speed at no-load

The copper loss versus torque curves in Fig. 7a show that below 120 Nm, the SPM has the lowest copper loss and at higher torques the IPM has the lowest copper loss. The IM generally has the highest copper loss versus torque curve.

The torque versus current curves in Fig. 7b show that the three machines have generally linear current versus torque characteristics over most of the operating range implying a dominant copper loss term of the form $k_{20}T^2$. The IM and IPM designs have a non-linear region at low current and the SPM design is non-linear at high currents.

The no-load power loss versus torque curves in Fig. 8 include iron losses and magnet losses where appropriate and have the general form $k_{02}\omega^2$. The SPM has the highest no-load loss, which at maximum speed is comparable to its copper loss at its continuous torque capability. This is due to a combination of the high magnet loss and the large stator current needed to field-weaken the large back-emf voltage (over three times rated voltage) at this speed. The IPM no-load loss at maximum speed is small (150 W) due to its relatively low back-emf voltage and the induction machine also has nearly zero electromagnetic losses. Note that bearing and windage losses are not included in this analysis.
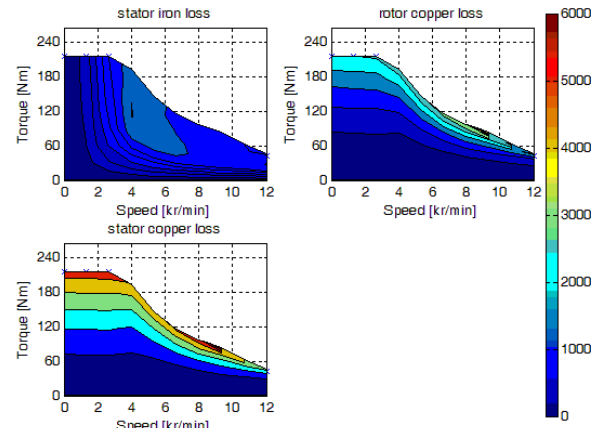
(a) IM
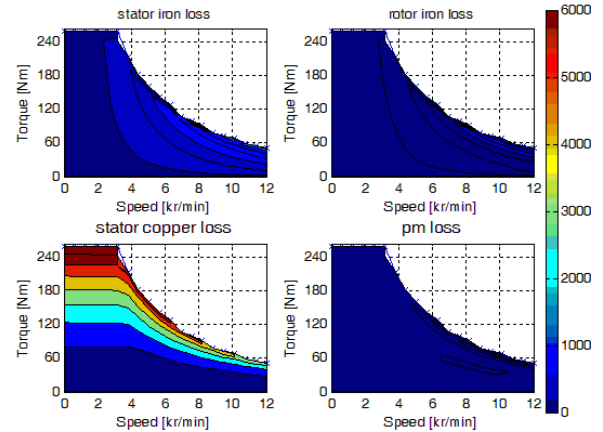
(b) IPM
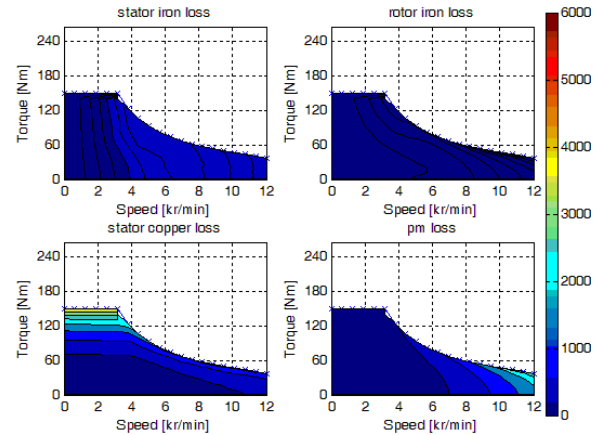
(c) SPM

Figure 9.   Contour plot loss breakdowns for the IM, IPM and SPM machines.

The power loss contours plotted on the torque versus speed and power versus speed plots in Fig. 6 can now be examined. It is also useful to refer to the loss breakdowns in Fig. 9 for the three machines which show contour plots of the stator iron and copper losses along with the different types of rotor losses plotted on axes of torque versus speed.

2796

The standstill copper loss curves in Fig. 7a correspond to the *y*-axis intercept and the no-load loss curves in Fig. 8 correspond to the *x*-axis intercept of the torque versus speed plots in Fig. 6. The differences in the no-load loss is clearly evident with the no-load loss being lower than 200 W over the entire speed range for IM and IPM designs while being much larger for the SPM design.

In the constant torque region of the torque-speed curves in Fig. 6, corresponding to speeds of approximately 3 kr/min or less, the power loss is dominated by copper losses and the contours would ideally be horizontal in a similar fashion to the stator copper loss plots in Fig. 9. In practice, speed-related losses such as iron and magnet losses cause these contours to slope downwards. The steepness of the slope of these contours corresponds to the ratio of the speed-related losses to the copper losses. Thus for the SPM the contours at 2 kr/min slope downwards more at low torques, corresponding to low copper loss, than at high torques where the copper loss is much larger.

In the constant power region of the power-speed curves in Fig. 6, that is between about 4 to 12 kr/min, the IM has almost horizontal power loss contours. That is, the power loss is proportional to output power and not greatly affected by speed. This implies the dominant power loss components in Fig. 9a (the stator and rotor copper losses) are proportional to output power. From Fig. 9b, the IPM power loss in this region is mainly due to stator copper and iron losses. The contours in Fig. 6 are fairly horizontal but have a small downwards slope, again implying a speed-related power loss. This could be partly due to the extra copper losses associated with field-weakening. The SPM has almost vertical power loss contours near the *x*-axis which implies that the speed-dependent losses are much larger than the power-dependent losses in this region. From Fig. 9c these are mainly due to stator iron and magnet losses.

Now consider the efficiency plots in the power versus speed plane in Fig. 6. For the IM, the nearly horizontal power loss contours in the constant power region result in matching horizontal efficiency contours. It has a rectangular peak efficiency (94%) region corresponding to medium to high speeds and medium output power. The IPM has a slightly higher peak efficiency (96%) and its efficiency contours match the slope of the power loss contours. It has a more triangular-shaped peak efficiency region corresponding to medium speeds and output powers. The SPM has a similar peak efficiency to the IPM but the high speed-dependent losses results in a smaller tear-drop-shaped maximum efficiency region. This occurs at low to medium speeds and medium output powers.

V.   Modelling Using Loss Functions

This section investigates the curve fitting of the calculated loss plots $P_L(T^m, \omega^n)$ in Fig. 6 using the sum of terms of the form $k_{mn}T^m\omega^n$ to examine its ability to reproduce both the loss and efficiency plots. The curve fitting is performed for the SPM and IPM machines.

Normalised loss terms of the following form are used in the curve fitting,
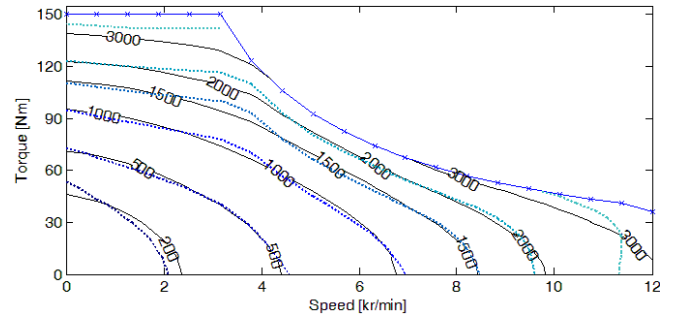
(a) curve fit of power loss contour plot using terms of the form $k_{mn}T^m\omega^n$
P_{loss}= -0.002 + 0.175 ω – 0.065 T + 0.181 ω² + 0.577 Tω + 0.697 T² + 0.443 ω³ – 0.542 Tω² – 1.043 T²ω + 0.942 T³ pu
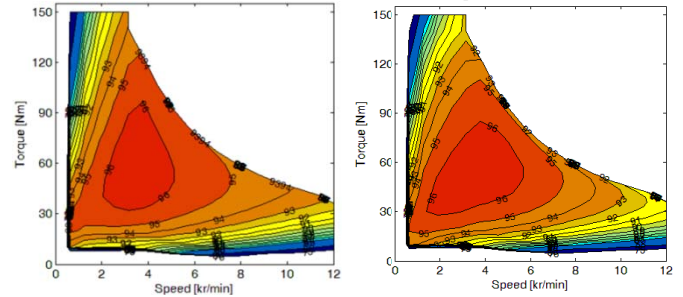
(b) curve fitted efficiency map   (c) actual (FEA) efficiency map

Figure 10. SPM curve fitted loss function and efficiency maps.

$$P_{loss}(T,\omega) = \sum k_{mn}\left(\frac{T}{T_b}\right)^m \left(\frac{\omega}{\omega_b}\right)^n \quad \text{pu} \qquad (7)$$

where the base torque T_b is 250 Nm, the base speed ω_b is 12 kr/min and the base power is equal to the maximum loss of 8 kW.

Fig. 10 uses terms where *m* and *n* have values of up to 3 to predict the loss behaviour of the surface PM machine and hence model its associated efficiency map. Fig. 10a shows the curve-fitted loss contours (colored lines) versus the actual (FEA) loss contours (black lines). The loss function model agrees well with that from FEA over a wide range but there are some discrepancies in the low and high loss values mainly at light loading or low speeds. Similarly, the efficiency map from the modelled loss function (Fig. 10b) shows a reasonable match with the FEA result (Fig. 10c).

All the machines discussed in this paper operate in two main regions in the torque-speed plane: constant torque and constant power. It is logical to consider the two operating regions separately as the control and hence performance of the machine is quite different. This is evident from the loss plot for the IPM machine in Fig. 6 where there is a definite change in the shape of the contours in the two regions.

Therefore, the curve-fitted loss for the interior PM machine is performed based on separate curve fits for the constant torque and for the constant power operating regions of the loss plot. The curve fitting based on single function over the whole operating region is also performed to compare the results. Fig. 11a is the two-function curve loss (color lines) against the actual loss (black lines). Figs. 11b-d compare the efficiency maps of the interior PM machine
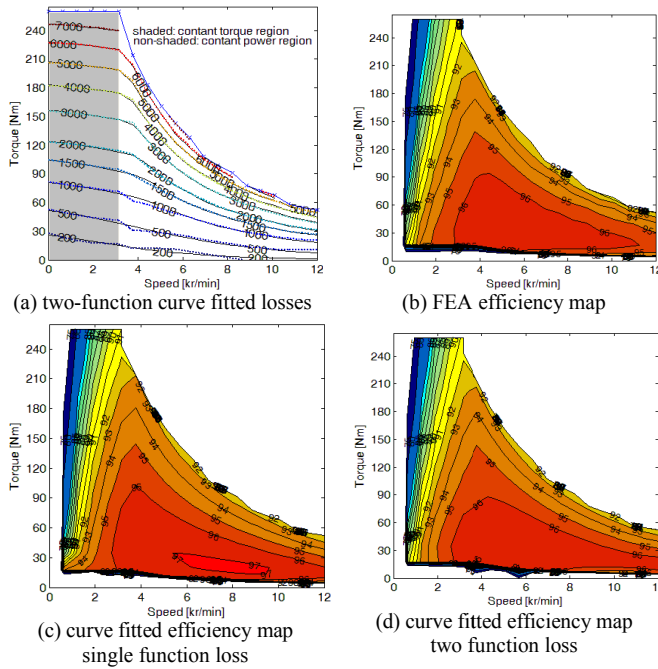
2797

Figure 11. IPM curve fitted loss function and efficiency maps

(a) two-function curve fitted losses

(b) FEA efficiency map

(c) curve fitted efficiency map single function loss

(d) curve fitted efficiency map two function loss

TABLE III.   NORMALISED LOSS COEFFICIENTS FOR SPM AND IPM MACHINES USING SINGLE FUNCTION MODELING. UPPER VALUES FOR SPM, LOWER VALUES FOR IPM.

	1	ω	ω^2	ω^3
T^3	**0.942**			
	0.339			
T^2	**0.697**	-1.043		
	0.103	**1.071**		
T	-0.065	**0.577**	-0.542	
	0.470	-1.022	**0.534**	
1	-0.002	0.175	0.181	**0.443**
	-0.033	0.239	-0.334	0.171
SPM / **IPM**	1	ω	ω^2	ω^3

TABLE IV.   NORMALISED LOSS COEFFICIENTS FOR IPM MACHINE USING TWO FUNCTION MODELING. UPPER VALUES FOR CONSTANT TORQUE, LOWER VALUES FOR CONSTANT POWER.

	1	ω	ω^2	ω^3
T^3	0.084			
	1.008			
T^2	**0.640**	-0.034		
	-0.944	**1.466**		
T	0.175	-0.028	**0.800**	
	0.958	-1.547	**0.728**	
1	-0.004	0.117	-0.316	0.131
	0.103	-0.647	**1.200**	-0.626
const. torque / **const. power**	1	ω	ω^2	ω^3

design and the lower value corresponds to the IPM design. Positive values which are greater than +0.3 are highlighted (in bold) as significant. It is interesting to note that there are some terms with large negative co-efficients e.g. for the SPM design, -1.043 for $T^2\omega$.

For the SPM, the most significant loss terms were of the form T^2, T^3, $T\omega$ and ω^3. For the IPM, the most significant terms were of the form T, T^3 $T^2\omega$ and $T\omega^2$. It was found that losses with coefficients $m + n > 3$ do not have much effect on the losses of these permanent magnet machines.

Table IV compares the normalised coefficients of the two loss functions used to model the interior PM machine in the constant torque and constant power operating regions. In the constant torque region the terms T^2 and $T\omega^2$ were most significant and in the constant power region the terms T, T^3, $T^2\omega$, $T\omega^2$ and ω^2 were the most significant.

VI.   THOR EXPERIMENTAL EFFICIENCY TESTING

Experimental loss and efficiency results are not available for the three 50 kW machines examined in this paper. It is thus planned to collect detailed experimental results from another traction machine. The machine called Thor is a 7.5 kW IPM machine designed for a small electric vehicle [11]. Its cross-section is shown in Fig. 12 and it uses a three-barrier design with ferrite magnets. It has a stator outer diameter of 170 mm and a stack length of 120 mm.

The experimental test arrangement is shown in Fig. 13. Two identical Thor motors are connected back-to-back for the performance testing. Presently no torque transducer is available on the test arrangement so the torque is estimated based on the commanded currents.

Fig. 14 shows the preliminary measured efficiency plot for the machine. It has a similar shape to that of the 50 kW IPM machine in Fig. 6 but has a slightly lower peak efficiency of 94% versus 96% but also a somewhat broader region for the peak efficiency.
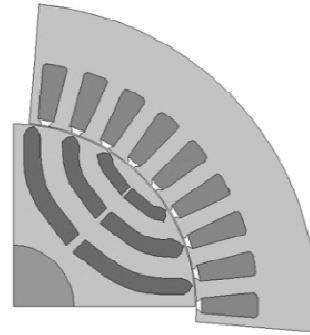

Figure 12. Sketch of the Thor machine cross-section. The actual rotor flux barriers are modified slightly to house the rectangular ferrite magnet blocks

based on FEA, single function curve-fitted, and two function curve-fitted, respectively. It is seen that the two function curve-fit provides a much better match with the actual efficiency map.

Table III lists the normalised coefficients of the $k_{mn}T^m\omega^n$ curve fit model for both surface and interior PM machines when a single function is used to model the entire operating range. For each cell, the upper value correspond to the SPM
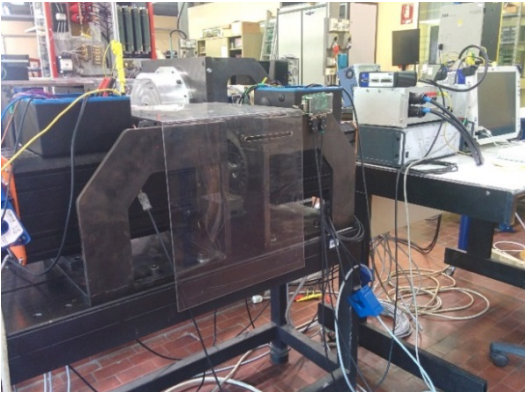
2798

Figure 13. Experimental setup: two identical Thor motors are connected back-to-back and mounted on C-frames. On the right-hand side are the current and temperature transducers and data logger.
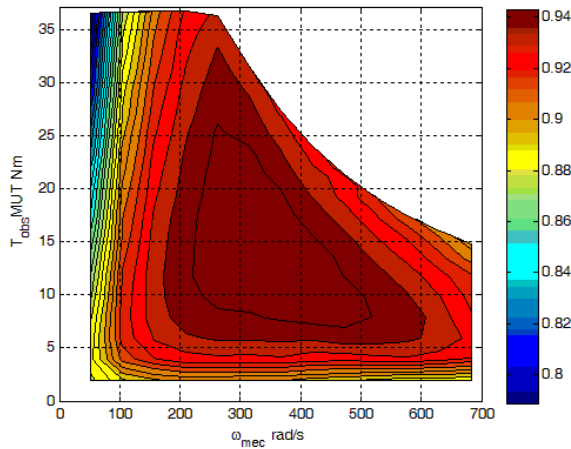

Figure 14. Preliminary measured efficiency map for Thor machine

VII. CONCLUSIONS

This paper has examined the calculation, modeling and interpretation of efficiency maps of electrical machines for example induction, interior permanent magnet and surface permanent magnet machines. The efficiency maps are calculated using an extensive finite-element based mapping of losses, torque and flux-linkage as a function of the d- and q-axis currents and speed.

The key results from this paper are as follows:

- it is shown that the power loss of a machine operating at a given torque T and speed ω can be represented as the sum of terms of the form $k_{mn}T^m\omega^n$ where m and n are integers;
- each of the above loss terms affects the shape of the total loss as a function of T and ω, and the shape of this total loss map determines the shape of the efficiency map;
- the most important loss terms can be estimated by analysis of the electrical machine and its control, and are different in the constant torque and field-weakening operating regions;
- curve fitting the loss map in the constant torque and constant power operating regions can be used to identify the major loss terms in the machine.

REFERENCES

[1] K. Kiyota, H. Sugimoto and A. Chiba, "Comparison of energy consumption of SRM and IPMSM in automotive driving schedules," Energy Conversion Congress and Exposition (ECCE), 15-20 Sept. 2012, pp. 853-860.

[2] S. S. Williamson, S. M. Lukic, and A. Emadi, "Comprehensive drive train efficiency analysis of hybrid electric and fuel cell vehicles based on motor-controller efficiency modeling," Power Electronics, IEEE Transactions on, vol. 21, pp. 730-740, 2006.

[3] X. Liu, D. Wu, Z. Q. Zhu, A. Pride, R. P. Deodhar and T. Sasaki, "Efficiency Improvement of Switched Flux PM Memory Machine Over Interior PM Machine for EV/HEV Applications," IEEE Trans. Magns, vol. 50, no. 11, pp. 1-4, Nov. 2014.

[4] C.-Z. Liaw, D. M. Whaley, W. L. Soong, and N. Ertugrul, "Investigation of inverterless control of interior permanent-magnet alternators," Industry Applications, IEEE Transactions on, vol. 42, pp. 536-544, 2006.

[5] X. Chen, M. Edington, R. Thornton, Y. Fang and Q. Peng, "Development Issues of an ISG PM Machine and Control System," International Conference on Power Electronics, Korea, 2007, pp. 922-929.

[6] G. Pellegrino, A. Vagati, P. Guglielmi, and B. Boazzo, "Performance Comparison Between Surface-Mounted and Interior PM Motor Drives for Electric Vehicle Application," Industrial Electronics, IEEE Transactions on, vol. 59, pp. 803-811, 2012.

[7] G. Pellegrino, A. Vagati, B. Boazzo, and P. Guglielmi, "Comparison of Induction and PM Synchronous Motor Drives for EV Application Including Design Examples," Industry Applications, IEEE Transactions on, vol. 48, pp. 2322-2332, 2012.

[8] Infolytica, "Core Loss and Efficiency Calculations", available: http://www.infolytica.com/ [accessed: 30 June 2015].

[9] P. Sergeant and A. Van den Bossche, "Segmentation of magnets to reduce losses in permanent-magnet synchronous machines," IEEE Trans. Magn., vol. 44, no. 11, pp. 4409–4412, Nov. 2008.

[10] L. Alberti, N. Bianchi, and S. Bolognani, "Variable-speed induction machine performance computed using finite-element," IEEE Trans. Ind. Appl., vol. 47, no. 2, pp. 789–797, Mar./Apr. 2011.

[11] Progetto Thor, available: http://www.thor.piemonte.it/progetto/ [accessed: 30 June 2015] (in Italian).

2799